Available online at www.sciencedirect.com
SCIENCE DIRECT®
Journal of Power Sources 146 (2005) 753–757
JOURNAL OF POWER SOURCES
www.elsevier.com/locate/jpowsour

Capacity degradation of lithium rechargeable batteries

J.P. Zheng [a,*], P.L. Moss [a], R. Fu [b], Z. Ma [b], Y. Xin [b], G. Au [c], E.J. Plichta [c]

[a] *Department of Electrical and Computer Engineering, Florida A&M University and Florida State University, Tallahassee, FL 32310, USA*
[b] *National High Magnetic Field Laboratory, Florida State University, Tallahassee, FL 32310, USA*
[c] *U.S. Army Communications-Electronics Command, Ft. Monmouth, NJ 07703, USA*

Available online 25 April 2005

Abstract

Li rechargeable cells made with structural arrangement Li/membrane/$Li_xV_2O_5$ were examined under different charge states using ac impedance, environmental scanning electron microscope (ESEM), transmission electron microscope (TEM) and the high-resolution nuclear magnetic resonance (NMR). These states include charged, discharged, and over cycled. The lowest internal resistance was obtained from the cell at charged state; the resistance increased when the cell was discharged; and the highest resistance was obtained from the cell at over-cycled state. From the ESEM and TEM studies, it was found that the surface of cathode electrode was porous initially; however, it was coated with an amorphous film and porous features had also disappeared from the cell at over cycled state. In addition, higher concentration of aluminum was found at the surface of the cathode electrode in over-cycled cells. From NMR studies, Li ion signals, which correspond to Li ions in the liquid electrolyte, on the surface of $Li_xV_2O_5$ cathode electrode, and inside the $Li_xV_2O_5$ cathode, were obtained. The mechanisms for capacity degradation and cycle lifetime of the cell are discussed.

Keywords: Capacity degradation; LiV_2O_5 cathode; Li rechargeable batteries

1. Introduction

A Li rechargeable battery is formed from three active components that include a metallic lithium (Li) anode, a lithium-ion-conducting electrolyte, and a lithium insertion cathode (such as $Li_xM_yO_z$; M = V, Mn, Co, Ni) [1–3]. During cell discharge and charge, Li is inserted into and extracted from the host structures of the cathode electrodes, respectively. The ideal electrode material and electrolyte for Li rechargeable batteries should have outstanding electrochemical performance and stable capacity upon extended cycle life. However, degradation on the anode, cathode electrodes, and electrolyte always occurs during the charge and discharge cycling. Various mechanisms that caused the capacity degradation and decreased cycle life of the battery were reported by different groups. For example, the decomposition of organic electrolytes with gas generation during charge and discharge cycling was obtained [4–7]. This process would result in depletion of the solvent in the electrolyte and deposition of Li [8] and other films [7] on the electrode surfaces. The depletion of the solvent and deposition of thin films developed in the batteries contributes toward the increase of battery impedance and ending of battery life. It was also found that the charge and discharge cycling of cathodes caused microstructural damage and cation disorder [9,10]. It was believed that breakdown of the oxide cathode material due to repeated lattice contraction and expansion appears to be an important failure mode in the oxide electrodes [10]. It was also reported that the dendritic electrodeposition of Li had been obtained in Li-polymer cells [11,12]. The Li dendritic growth would eventually short the battery.

2. Experimental

Panasonic® vanadium pentoxide (V_2O_5) Li-rechargeable batteries were used as experimental samples. The button cell batteries were made with Li (anode)/membrane/$Li_xV_2O_5$ (cathode), and were rated at 30 mA h. The aluminum (Al)

* Corresponding author. Tel.: +1 850 410 6464; fax: +1 850 410 6479.
E-mail address: zheng@eng.fsu.edu (J.P. Zheng).

0378-7753/$ – see front matter © 2005 Elsevier B.V. All rights reserved.
doi:10.1016/j.jpowsour.2005.03.076

mesh and stainless steel bottom case of the button cell were used as the current collectors for anode and cathode electrodes, respectively. The cells are 23 mm in diameter and 2.0 mm in thickness.

An Arbin battery test system was used for charge and discharge cycling of cells. During the charge cycle, a constant voltage mode of 3.4 V was used and during discharge cycle, a constant current mode at 10 mA was used. Three different samples for ac impedance spectral, microscopic, and NMR studies were prepared as follows: one charged cell was charged to 3.4 V at a constant voltage mode; one discharged cell was discharged to 2.1 V at a constant current (10 mA) mode; and one over-cycled cell was continuously charged and discharged until the cell had the capacity close to zero. A Solartron electrochemical measurement unit (model 1280B) was used to measure the ac impedance spectra in a frequency range from 0.01 Hz to 20 kHz at room temperature. During ac impedance measurements, a sinusoidal source with an amplitude of 10 mV superimposed on a dc bias voltage was applied to the cell. The dc voltages were 3.4 and 2.1 V for charged and discharged cells, respectively. An integral step of 2 s was also used to increase the accuracy at each frequency point to offset the error due to the presents of noise in the lines connecting the spectrometer to the battery.

After ac impedance spectral study, these cells were then opened, and the $Li_xV_2O_5$ cathode electrode materials were removed from cells in a glove box filled with argon gas for microscopic and NMR studies.

An environmental scanning electron microscope (ESEM) was used for imaging the surface morphology of electrodes. The energy dispersive X-ray spectroscope (EDX) built into the ESEM system was employed to analyze the chemical composition of the electrode. A Jeol-2010 transmission electron microscope (TEM) operated at 200 kV and selected area electron diffraction (SAED) built into the TEM system were used to investigate the microstructures of the cathode materials including particles morphology and crystalline structures.

The ^{7}Li NMR measurements were performed on Bruker DMX-600 spectrometers ($B_0 = 14.1$ T) with ^{7}Li NMR frequency of 233.31 MHz. The ^{7}Li spin-lattice relaxation times were measured in a temperature range of 220–300 K.

3. Results and discussion

Fig. 1 shows the charge and discharge capacities as a function of number of cycle at about 25 °C. The battery was cycled in a voltage range from 2.1 to 3.4 V. It can be seen that the initial capacity of the cell was about 35 mA h; however, after 26 cycles, the capacity reduced to less than 15% of the initial capacity.

Fig. 2 shows Nyquist plot of three cells at 25 °C. The Nyquist plot for the charged cell shows a small semi circle in the frequency range from 0.794 Hz to 20 kHz and a linear plot at an angle of 52° with frequency range from 0.01 to 0.794 Hz. The semi circle in this plot represents the charge transfer at

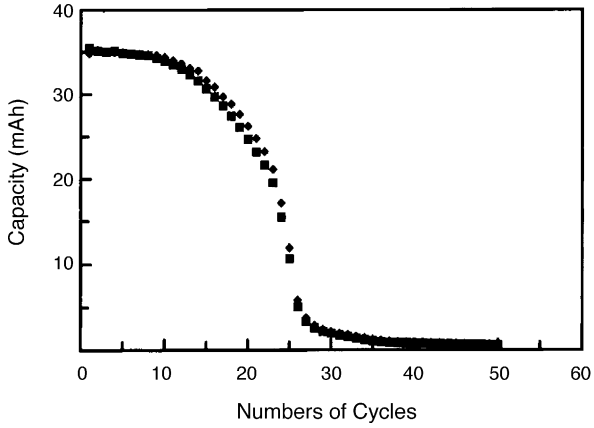

Fig. 1. Capacities of the cell as a function of cycle numbers during discharge process at 25 °C. Symbols of (♦) and (■) represent charge and discharge capacities.

the electrolyte/electrode interface and the linear portion of this plot (0.01 to ~0.794 Hz) represents the diffusion of Li into the $Li_xV_2O_5$ structure or break of phase boundaries in the structure. Upon closer examination it can be seen at a high frequency of 20 kHz there was an electrolyte resistance of about 3.1 Ω. The charge transfer resistance at the electrolyte electrode interface can be determined by Z′ at 0.794 Hz, and was approximately 12.2 Ω–3.1 Ω = 9.1 Ω. The low frequency point (~0.01 Hz) represents the diffusion of Li in and out of the $L_xV_2O_5$ structure. The Nyquist plot for discharged cell shows an electrolyte resistance of the same value as that of the charged cell. However, the charge transfer resistance for discharged cell was greater than 100 Ω. The impedance at low frequency (0.01 Hz) was also much greater than that for charged cell. The increase in charge transfer resistance and impedance at low frequency can be understood by the fact that the concentrations of Li ions in the

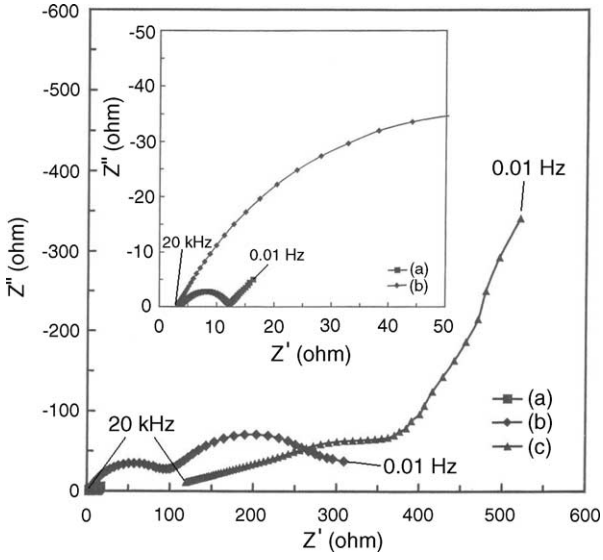

Fig. 2. The Nyquist plot of cells at (a) charged, (b) discharged, and (c) over-cycled states in the frequency range from 0.01 Hz to 20 kHz at room temperature.

electrode surface region and in $Li_xV_2O_5$ were high and as a result the diffusion of Li ions in and out of the surface region and the structure were low. The Nyquist plot from over-cycled cell shows a dramatic increase in the electrolyte resistance at 20 kHz which is directly related to a decrease in ionic conductivities. This decrease in conductive indicates a decrease in cycle life. At both high and low frequencies the transport of Li ions flowing from the anode to the $Li_xV_2O_5$ structure was very low.

In order to closely examine the cathode electrodes at discharged states, ESEM system was used to study the surface morphology and chemical composition. Fig. 3a and b show surface morphologies of $Li_xV_2O_5$ cathode electrodes at the interface with membrane for cells from charged and over cycled states, respectively. It can be seen from Fig. 3a that the electrode was formed with particles in microsize; the boundary between particles could clearly be seen. The voids and grooves up to 10 μm could also be observed. Similar surface morphology was obtained from the cathode electrode of the discharge cell. However, from Fig. 3b for an over cycled cell, the boundary between particles could not be identified.

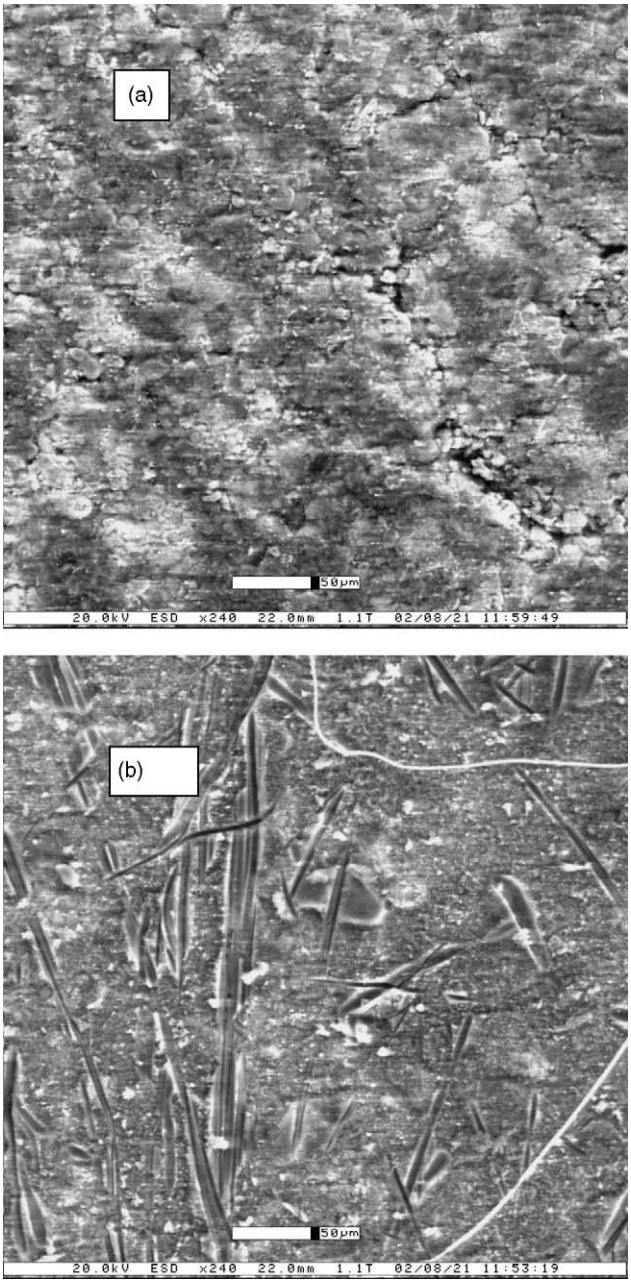

Fig. 3. ESEM images of cathode surfaces from (a) charged and (b) over-cycled cells. The surface faced to membrane in the cell.

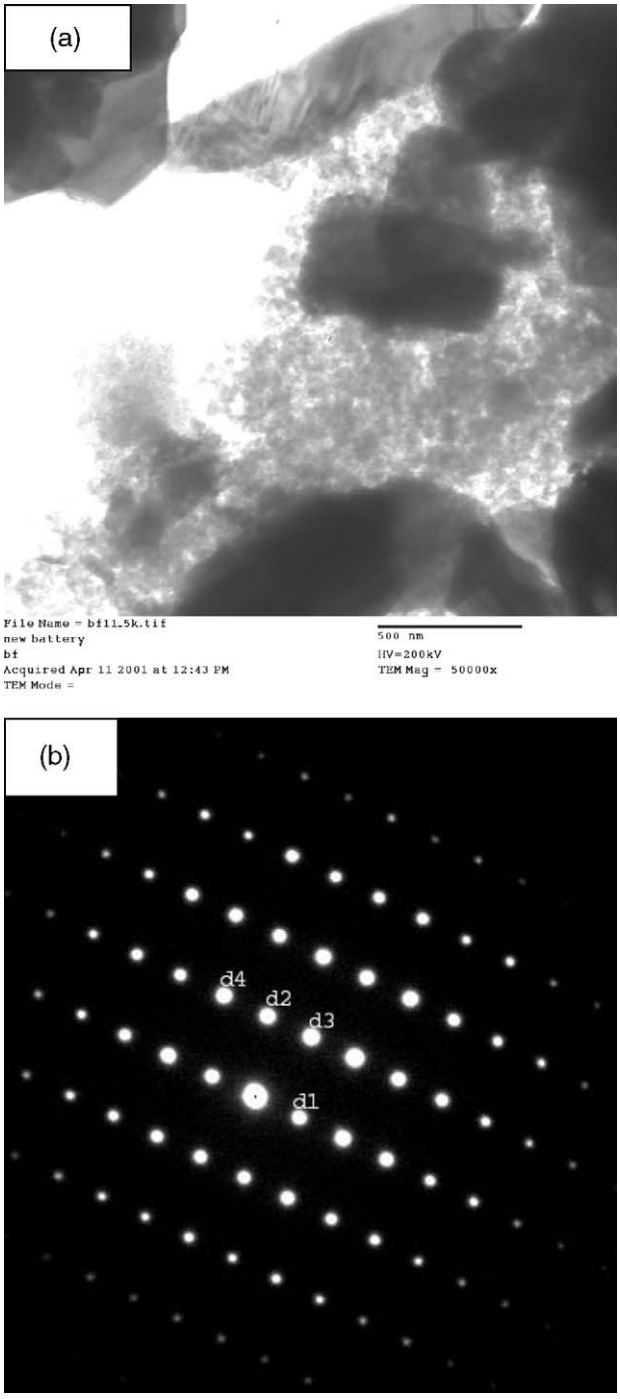

Fig. 4. (a) TEM image of cathode material from a charged cell, and (b) SAED pattern from the large particle.

The voids and grooves had also disappeared. The lines on the surface are traces of membrane surface.

The chemical compositions at the cathode surface were analyzed using EDX. The system can only detect elements that are heavier than oxygen; therefore, Li and other components from the electrolyte could not be identified. It was found that the intensity of Al signals from the over-cycled cell was higher than that from charged cell. The result indicated that the Al was deposited on the surface of cathode during the charge and discharge cycle; the only source for Al in the cell is the current collector from the Li anode electrode. The Al must have been dissolved in the electrolyte before the deposition on the cathode electrode. The Al distribution inside the cathode electrode was also investigated by mapping the Al signal on a cross-section of cathode electrode. It was found that in general the Al concentration inside the electrode was much lower than that on the surface of electrode, and was quite uniformly distributed inside electrode. This observation is reasonable, since the deposition would occur on surface and along the boundary of particles. Therefore, where the voids and grooves existed, it would have high concentration of Al.

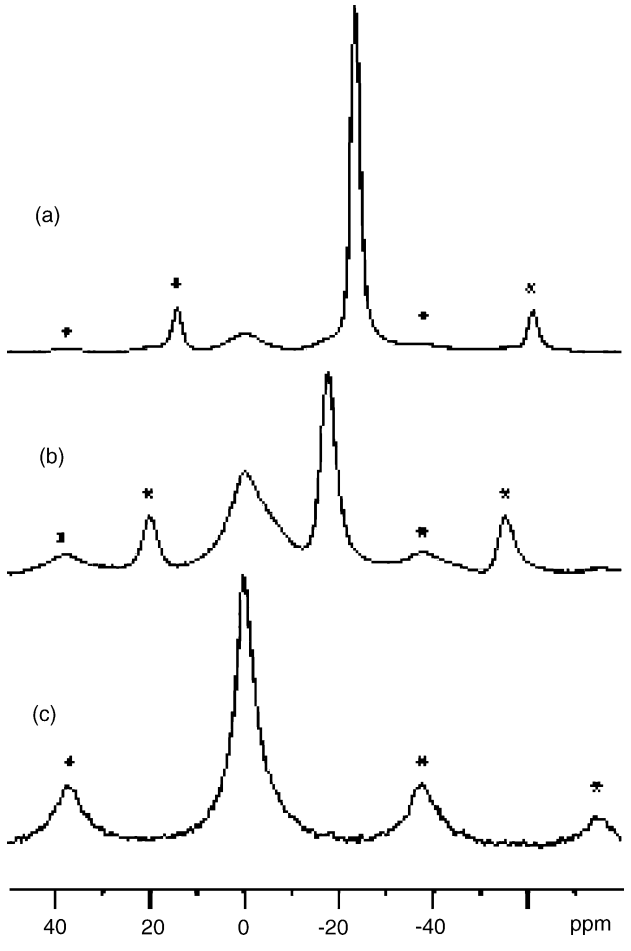

Fig. 5. The ^{7}Li NMR spectra of $Li_xV_2O_5$ cathode materials from three different charge states: (a) discharged state, (b) charged state, and (c) over cycled state. The asterisks indicate the spinning sidebands.

TEM was also used to image particles in the cathode electrode. Fig. 4 shows a TEM image of the cathode material from a charged cell. From TEM images, we can see that two different groups of materials were found from the electrode. The majority material was formed with large particles in the order of μm. The SAED patterns indicated that large particles were single crystalline phase of $Li_xV_2O_5$, close to the crystal structure of V_2O_5. Amorphous regions containing small particles were also present, these amorphous regions have high amount of Al from the EDX analysis. From both TEM and EDX results, there is no ascertainable difference in the general features among three cells at different charged states including over-cycled state. It indicates that no microstructural crash or damage occurred in V_2O_5 crystals.

Fig. 5 shows the ^{7}Li NMR spectra for the $Li_xV_2O_5$ samples at the different charge states. Clearly, there exists a broad peak at −0.4 ppm in the spectra. For discharged state, the resonance at −23.6 ppm has much greater intensity than that at −0.4 ppm and such can be attributed to the excess Li ions inserted into the $Li_xV_2O_5$ cathode electrode during the discharge process. For the charged state, the peak intensity at −17.6 ppm is on the same order of that at −0.4 ppm. For the over cycled state, no resonance signal is observed except one at −0.4 ppm. From temperature dependence of ^{7}Li NMR spectra as well as the spin–lattice relaxation times measurements, it was found that there were two components in the resonance at −17.0 to −23.0 ppm as shown in Fig. 6. The sig-

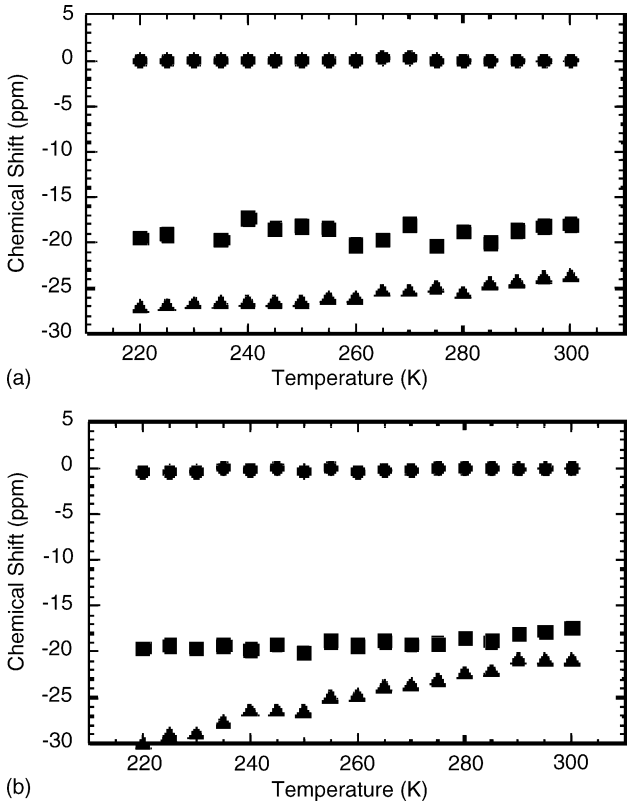

Fig. 6. Temperature dependence of the ^{7}Li chemical shifts for the $Li_xV_2O_5$ cathode materials at (a) the discharged and (b) the charged states.

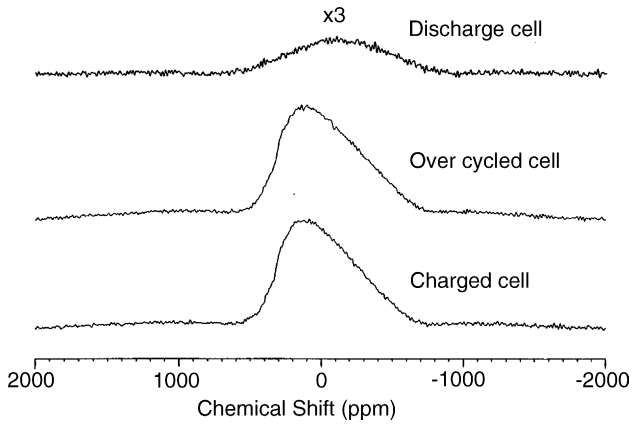

Fig. 7. Static ^{51}V NMR spectra of different $Li_xV_2O_5$ cathodes at room temperature.

nal at −17.0 is almost temperature independent as shown in Fig. 6, for both the charged and discharged states. This resonance peak cannot be from Li-metal because the Knight shift for metallic lithium is typically in the range of 250–360 ppm [13,14]. While the signal at −17.0 ppm has similar intensity with respect to the peak intensity at −0.4 ppm for both the charged and discharged states, it is thus attributed to the Li ions on the surface of the V_2O_5 host, since it is reasonable to believe that the V_2O_5 hosts in the different charge states have similar surface area.

The ^{51}V NMR spectral measurements have clearly shown the transition from V^{5+} and V^{4+} states when Li concentration increased in $Li_xV_2O_5$ structure. Fig. 7 shows that broad signals were obtained from three samples with different charge states. The broad signal is due to the quadrupolar effect. Similar signals were obtained from samples from the charged and over cycled cells. For both samples, the Li concentration in $Li_xV_2O_5$ was so low that V^{5+} species were over dominating. However, for sample from the discharge cell, V^{4+} and perhaps even V^{3+} species increased with increasing the Li concentration. The paramagnetic V^{4+} and V^{3+} ions are responsible for the loss of the intensity in ^{51}V NMR signal [15,16].

4. Conclusions

The TEM image and SEAD study obtained single crystalline V_2O_5 particles in cathode electrode for all charged states. There is almost identical ^{51}V NMR spectra also obtained from charged and over-cycled $Li_xV_2O_5$ samples, which suggested that the capacity degradation and cycle life of Li–$Li_xV_2O_5$ cells was not due to the degradation such as structure damage or cation disorder of the cathode. Also, from the high-resolution ^{7}Li NMR spectra, two groups of Li were obtained from the cathode electrode of charged and discharged cells, they were located inside and outside of the V_2O_5 structure; however, only the Li located outside of V_2O_5 structure was obtained from the cathode electrode of over cycled cell. After considering all experimental observations, we suggested that the capacity degradation and cycle life of Li–$Li_xV_2O_5$ cells are due to the decomposition of organic electrolyte during charge and discharge cycling. This process would result in depletion of the solvents in the electrolyte and also deposition of Li, Al, and other materials on the surface of the cathode electrode, which reduced the porosity of the electrode. The depletion of the solvent and deposition of thin film on the cathode electrode caused the increase of cell impedance and ending of the battery life. The degradation mechanism for Li–$Li_xV_2O_5$ cells is similar to the for Li–MoS_2 cells [6].

Acknowledgements

This work was partially supported by US Army Communications–Electronics Command. RF thanks Program Enhancement Grant (PEG) (Project #550240537) from Florida State University. XY thanks NHMFL funded by NSF under cooperative agreement DMR-0084173 and the State of Florida.

References

[1] P. Baudry, S. Lascaud, H. Majastre, D. Bloch, J. Power Sources 68 (1997) 432–435.
[2] K. Murata, S. Izuchi, Y. Yoshihisa, Electrochim. Acta 45 (2000) 1501–1508.
[3] D. Fauteux, A. Massucco, M. McLin, M. van Buren, J. Shi, Electrochim. Acta 40 (1995) 2185–2190.
[4] Z.X. Shu, R.S. McMillan, J.J. Murray, J. Electrochem. Soc. 140 (1993) 922–927.
[5] E. Cattaneo, J. Ruch, J. Power Sources 43–44 (1993) 341–347.
[6] K. Kumai, T. Ikeya, K. Ishihara, T. Iwahori, N. Imanishi, Y. Takeda, O. Yamamoto, J. Power Sources 70 (1998) 235–239.
[7] H. Yoshida, T. Fukunaga, T. Hazama, M. Terasaki, M. Mizutani, M. Yamachi, J. Power Sources 68 (1997) 311–315.
[8] D. Aurbach, E. Zinigrard, H. Teller, P. Dan, J. Electrochem. Soc. 147 (2000) 1274–1279.
[9] H. Wang, Y.I. Jang, B. Huang, D. Sadoway, Y.M. Chiang, J. Power Sources 81–82 (1999) 594–598.
[10] J.H. Lee, J.K. Hong, D.H. Jang, Y.K. Sun, S.M. Oh, J. Power Sources 89 (2000) 7–14.
[11] C. Brissot, M. Rosso, J.N. Chazalviel, S. Lascaud, J. Power Sources 81–82 (1999) 925–929.
[12] C.W. Kwon, S.E. Cheon, J.M. Song, H.T. Kim, K.B. Kim, C.B. Shin, S.W. Kim, J. Power Sources 93 (2001) 145–150.
[13] G.C. Carter, L.H. Bennett, D.J. Kahan, Metallic Shifts in NMR: A Review of the Theory and Comprehensive Critical Data Compilation of Metallic Material. Part I, Pergamon Press, New York, 1977.
[14] F. Beuneu, P. Vajda, O.J. Zogal, J. Nucl. Instrum. Meth. Phys. Res. B141 (1998) 241.
[15] A.A. Shubin, O.B. Lapina, E. Bosch, J. Spengler, H. Kuozinger, J. Phys. Chem. B 103 (1999) 3138.
[16] O.B. Lapina, A.A. Shubin, A.V. Nosov, E. Bosch, J. Spengler, H. Kuozinger, J. Phys. Chem. B 103 (1999) 7599.